



## Preparation of Mn-Zn ferrite nanoparticles and their silica-coated clusters: Magnetic properties and transverse relaxivity



Ondřej Kaman<sup>a,\*</sup>, Jarmila Kuličková<sup>a</sup>, Vít Herynek<sup>b</sup>, Jakub Koktan<sup>a,c</sup>, Miroslav Maryško<sup>a</sup>, Tereza Dědourková<sup>a,d</sup>, Karel Knížek<sup>a</sup>, Zdeněk Jiráček<sup>a</sup>

<sup>a</sup> Institute of Physics, AS CR, Cukrovarnická 10, 162 00 Praha 6, Czech Republic

<sup>b</sup> Institute for Clinical and Experimental Medicine, Vídeňská 1958/9, 140 21 Praha 4, Czech Republic

<sup>c</sup> University of Chemistry and Technology, Prague, Technická 5, 166 28 Praha 6, Czech Republic

<sup>d</sup> University of Pardubice, Doubravice 41, 532 10 Pardubice, Czech Republic

### ARTICLE INFO

#### Keywords:

Magnetic nanoparticles  
Mn-Zn ferrite  
Hydrothermal synthesis  
Magnetic resonance imaging  
Transverse relaxivity

### ABSTRACT

Hydrothermal synthesis of  $\text{Mn}_{1-x}\text{Zn}_x\text{Fe}_2\text{O}_4$  nanoparticles followed by direct encapsulation of the as-grown material into silica is demonstrated as a fast and facile method for preparation of efficient negative contrast agents based on clusters of ferrite crystallites. At first, the hydrothermal procedure is optimized to achieve strictly single-phase magnetic nanoparticles of Mn-Zn ferrites in the compositional range of  $x=0.2-0.6$  and with the mean size of crystallites  $\approx 10$  nm. The products are characterized by powder X-ray diffraction, X-ray fluorescence spectroscopy, and SQUID magnetometry, and the composition close to  $x=0.4$  is selected for the preparation of silica-coated clusters with the mean diameter of magnetic cores  $\approx 25$  nm. Their composite structure is studied by means of transmission electron microscopy combined with detailed image analysis and magnetic measurements in DC fields. The relaxometric studies, performed in the magnetic field of  $B_0=0.5$  T, reveal high transverse relaxivity ( $r_2(20^\circ\text{C})=450\text{ s}^{-1}\text{ mmol}(\text{Me}_3\text{O}_4)^{-1}\text{ L}$ ) with a pronounced temperature dependence, which correlates with the observed temperature dependence of magnetization and is ascribed to a mechanism of transverse relaxation similar to the motional averaging regime.

### 1. Introduction

Applications of magnetic nanoparticles in medicine, biological research and biotechnology have relied mainly on iron oxide cores, whose main advantages are the low toxicity and compatibility with natural metabolic pathways, ease of preparation by diverse methods including biomineralization, extensive knowledge of properties, and low cost of their production. However, some criticism of iron oxide nanomaterials has been raised, pointing out that their magnetic properties can hardly fulfil the demanding requirements of certain applications [1]. The well-known example is magnetically fluid hyperthermia (MFH), a method of cancer treatment through heat generated by magnetic nanoparticles in an alternating magnetic field, where possible overheating of a healthy tissue surrounding tumor constitutes a significant risk. Although some invasive thermometry could be used to monitor temperature distribution during the hyperthermia intervention, an attractive solution has been offered by the so-called self-regulated hyperthermia, that utilizes magnetic nanoparticles with Curie temperature adjusted just above the desired applica-

tion temperature [2,3]. For such type of magnetic particles, a thorough optimization of the heating efficiency and its self-regulation control has to be performed [4]. Apart from an account of classical relations in the evaluation of magnetic and frictional losses (see, e.g. [5]), an empirical approach seems to be indispensable for practical application since varying and strongly non-adiabatic conditions occur within biological systems owing to the circulation of body fluids and efficient thermo-regulation [6]. Another example is the use of magnetic nanoparticles as contrast agents for magnetic resonance imaging (MRI), where again, the binary iron oxides do not reach the optimum performance (e.g., iron oxides do not reach as high magnetization as certain ferrites [7]). Since the properties of magnetite, maghemite, and mixtures thereof can be varied only in a narrow range and mostly by their size and shape, more efficient tuning of magnetic properties is only possible in ternary oxides and in more complex systems by varying their chemical composition.

As regards the self-regulated heating mediators for MFH and contrast agents for MRI, the perovskite manganites and Zn-containing spinel ferrites were considered as promising nanoparticle systems to

\* Corresponding author.

E-mail address: [kamano@seznam.cz](mailto:kamano@seznam.cz) (O. Kaman).

replace the simple iron oxides. According to the comparative study of cytotoxicity of two selected representatives, specifically silica-coated nanoparticles of  $\text{La}_{1-x}\text{Sr}_x\text{MnO}_3$  manganite and  $\text{Mn}_{1-x}\text{Zn}_x\text{Fe}_2\text{O}_4$  ferrite, the latter showed superior properties [8]. Moreover, the composition of Mn-Zn ferrite nanoparticles can be optimized to increase the magnetization by a better balance between the antiferromagnetically coupled octahedral and tetrahedral sublattices, and by this virtue the particles exhibit also high transverse relaxivities,  $r_2$ , which is important for development of efficient contrast and labelling agents for MRI. In particular, significant contrast enhancement in MRI was reported by Jang et al. [7] who prepared single-crystalline 15 nm sized  $\text{Mn}_{1-x}\text{Zn}_x\text{Fe}_2\text{O}_4$  nanoparticles and found the maximum relaxivity as well as a corresponding maximum of magnetization for the composition  $\text{Mn}_{0.6}\text{Zn}_{0.4}\text{Fe}_2\text{O}_4$ .

Importantly, the transverse relaxation depends not only on magnetization but also on extrinsic properties, namely on the size of nanoparticles, their clustering, and surface coating, whose suitable adjustment might further increase the contrast effect. Similarly to different regimes of the transverse relaxation that were inferred for a system of well dispersed magnetic nanoparticles in relation to their size and characteristic diffusion time of water molecules (see, e.g. [9] for a brief overview supplemented by experimental data), an analogy exists for clusters of magnetic particles [10,11]. Taking a given size of magnetic nanoparticles (up to a certain limit), further increase of  $r_2$  can be accomplished by their well-controlled clustering, which was supported by a detailed experimental study very recently [12].

Several routes have been employed for the preparation of Mn-Zn ferrite nanoparticles, providing different materials in terms of the particle size distribution and cation distribution between the two sublattices, which both affects their magnetic behaviour. However, the synthetic procedure employed also determines surface properties of the resulting particles. The traditional approach utilized coprecipitation [13,14], sol-gel processes [15,16], and their derivatives [17], whereas the recent efforts have been devoted particularly to the synthesis of Mn-Zn ferrite nanocrystallites by the thermal decomposition [7,18], which became a general method for the preparation of single-crystalline monodisperse ferrite nanoparticles with bulk-like properties. The success of this technique originated from the efficient separation of the nucleation and the crystal growth of particles together with precise control of the kinetics, which enabled the preparation of monodisperse nanoparticles of various shapes including spheres, cubes, corner-grown cubic, and star-like shapes [19].

Nonetheless, the thermal decomposition procedure is experimentally complicated and employs expensive reactants. Further, the synthesis of strictly monodisperse nanoparticles involves cumbersome optimization of reaction conditions, and the as-prepared particles are capped by hydrophobic layer of surfactants and require specific procedures for solubilisation in water [20–22]. In contrast, the hydrothermal synthesis, starting with an aqueous solution of simple metal salts like chlorides or oxo-salts, offers a very facile, fast, and low-cost procedure.

The early reports on the hydrothermal synthesis of Mn-Zn ferrite nanoparticles revealed that the pH control is crucial for well-controlled synthesis of single-phase products since manganese is not completely precipitated at lower pH, but zinc might be considerably dissolved to  $[\text{Zn}(\text{OH})_4]^{2-}$  under highly alkaline conditions. Such preferential loss of divalent metal cations impairs the stoichiometry of the precipitated precursor, and as a result, hematite can be formed as an additional phase [23,24]. The typical as-grown ferrite nanoparticles prepared by the simple hydrothermal synthesis show some degree of aggregation [23], but if desired, they might be dispersed in water by conventional techniques.

The present study takes an advantage of the facile hydrothermal route optimized to achieve single-phase  $\text{Mn}_{1-x}\text{Zn}_x\text{Fe}_2\text{O}_4$  ferrite nanoparticles. Several samples of Mn-Zn ferrite nanoparticles of different compositions are prepared and analysed by powder X-ray diffraction

(XRD) and SQUID magnetometry. The as-prepared particles of the composition  $x=0.42$ , selected for their magnetic behaviour, are coated with silica. The composite structure of the resulting product is studied by transmission electron microscopy and probed by magnetic measurements. The relaxometric measurements are carried out to evaluate the contrast potential of the coated particles, and the temperature dependence of the transverse relaxivity is analysed to acquire a better insight into the mechanism of transverse relaxation.

## 2. Experimental details

### 2.1. Synthesis

#### 2.1.1. $\text{Mn}_{1-x}\text{Zn}_x\text{Fe}_2\text{O}_4$ ferrite cores (MZF(x))

Stock solutions of manganese(II) nitrate, zinc nitrate, and iron(III) nitrate slightly acidified with nitric acid were used as starting materials, after their concentrations had been determined by chelatometric titrations. Appropriate amounts were combined in the molar ratio Mn: Zn: Fe=(1-y): y: 1.80, where  $y=0.20, 0.30, 0.40, 0.50, 0.60$ , to reach the total metal content of 5.6 mmol, and the resulting solution was concentrated *in vacuo*. Further, the solution was deoxygenated and under inert atmosphere transferred into a Berghof DAB-2 pressure vessel equipped with a 50 mL Teflon insert. Magnetic stirring was applied, and pH of the solution was adjusted to 10.0 by adding  $\approx 2$  M sodium hydroxide solution, which led to formation of brown precipitates. The so-obtained mixture was subjected to the hydrothermal treatment under autogenous pressure at 180 °C for 12 h. The filling volume was 50%, and magnetic stirring was applied during the whole synthesis. The so-obtained product was washed several times with water and ethanol, and was dried at 110 °C on air. Typical amount prepared in a single batch was 430 mg.

#### 2.1.2. Silica-coated nanoparticles

As-prepared nanoparticles of the  $y=0.40$  product (300 mg) were treated with ice-cold 1 M nitric acid in an ultrasound bath for 15 min and separated by centrifugation. Subsequently, similar treatment with ice-cold 0.1 M citric acid followed. One washing cycle in water was applied, and the particles were redispersed in 20 mL water alkalized with ammonia by an ultrasound probe. The stabilized particles were transferred into the mixture of ethanol (675 mL), water (160 mL), and ammonia (45 mL) in 1 L round bottom flask placed in an ultrasound bath whose temperature was stabilized at 60 °C by an external heating circulator. At first, both ultrasound agitation and mechanical stirring were applied, and tetraethoxysilane (8.77 mL) was gradually added during 10 min. Then the ultrasound sonication was discontinued, and the mixture was stirred at 60 °C for 4 h. Thereafter, heating was terminated, and stirring continued overnight. The product was separated via centrifugation and thoroughly washed with ethanol and water. Size fractionation was carried out by repeated differential centrifugation at 1860 rcf for 15 min in three cycles, when the supernatant was collected, and the residue was recycled for a following cycle. Finally, the combined supernatants were fractionated again at 1860 rcf for 15 min.

### 2.2. Characterizations

The phase composition and crystal structure of ferrite cores were analysed by means of XRD (X-ray powder diffraction) with  $\text{CuK}\alpha$  line using a Bruker D8 diffractometer. The phase identification was based on the data from ICSD, and the diffraction patterns were analysed by the Rietveld method in the FULLPROF program. The mean crystallite size  $d_{\text{XRD}}$  was evaluated from peak broadening for which the Thompson-Cox-Hastings pseudo-Voigt profile was applied to separate the strain and size contributions. The instrumental profile was determined on a strain-free tungsten powder with crystallite size of 9.4  $\mu\text{m}$ . The accurate chemical composition of bare cores was analysed

by XRF (X-ray fluorescence spectroscopy) with an Axios spectrometer.

The morphology and size of coated particles was studied by the transmission electron microscope Philips CM 120. The size distribution was determined through image analysis of 200 particles for which the projected area of the whole coated particle  $S_p$  and its magnetic core  $S_c$  were accurately measured in the ImageJ software. Similarly, 200 crystallites were characterized by projected areas  $S_i$ . The diameter of the coated particles,  $d_p$ , the diameter of their cores,  $d_c$ , and the diameter of crystallites,  $d_i$ , were estimated according to the following approximations:  $d_j = \sqrt{4S_j/\pi}$ , where where  $j = i, c, p$ .

Magnetic properties were probed by SQUID magnetometry employing a Quantum Design MPMS XL system. The experiments involved measurement of hysteresis loops at 5 and 300 K. The zero-field-cooled (ZFC) and field-cooled (FC) susceptibilities were measured at the magnetic field intensity  $H=20$  Oe. Thorough demagnetization of the SQUID magnetic was applied prior to the ZFC measurement to remove remnant fields from the system. To allow a comparison with the relaxivity data taken on the coated sample (see Section 2.3.), additional magnetization measurements were performed on coated-particles at  $H=5$  kOe ( $B_0=0.5$  T) in the range of 273–348 K (0–75 °C).

### 2.3. Relaxometric studies

The concentration of coated particles in an aqueous suspension intended for relaxometry was determined through the chemical analysis of iron by atomic absorption spectroscopy (AAS) with flame atomization. The mineralization of samples involved treatment by hydrofluoric acid and nitric acid, whereas hydrogen peroxide was added to reduce all manganese to  $Mn^{2+}$ . The standard addition method was applied to suppress any matrix effects, and measurement was carried out at  $\lambda=248.3$  nm in an acetylene-air flame. The concentration of the suspension was adjusted to  $0.094$  mmol( $Me_3O_4$ )  $L^{-1}$  for the relaxometric measurements. The transverse relaxivity  $r_2$  was measured in the magnetic field of  $B_0=0.5$  T by a Bruker Minispec relaxometer. A modified CPMG (Carr-Purcell-Meiboom-Gill) multi-echo sequence was employed with technical parameters specified in Ref. [25]. The temperature dependence of  $r_2$  was obtained by stabilization of the measured sample by an external water bath in the range 5–70 °C. The actual temperature was measured directly in the suspension, and the probe was removed just before each acquisition.

## 3. Results and discussion

### 3.1. Synthesis, structure and morphology

The XRD analysis of bare ferrite cores, illustrated by diffraction patterns of selected samples in Fig. 1a, evidenced that single-phase products of spinel structure with the symmetry  $Fd\bar{3}m$  had been prepared in the entire range of studied composition  $x \approx 0.2-0.6$ . Their crystal structure was refined by Rietveld analysis based on the structure with the ICSD code 28515 as a reference. The cubic lattice parameter  $a$  and the mean size of crystallites are summarized in Table 1 together with the accurate chemical composition determined by XRF. The lattice parameter is linearly decreasing with the content of zinc (see also the unit cell volume in the inset of Fig. 1), following the Vegard's law, since the  $Zn^{2+}$  (ionic radius  $0.74$  Å) substitutes larger sized  $Mn^{2+}$  ( $0.83$  Å). The mean size of crystallites is practically the same for all the samples ( $d_{XRD} \approx 10$  nm), except for slightly increased size of crystallites with the lowest zinc content ( $d_{XRD}=14$  nm).

As regards the hydrothermal synthesis of  $Mn_{1-x}Zn_xFe_2O_4$  ferrite cores, it is worth mentioning that the chemical composition of prepared samples reflected tightly the molar ratio of Mn to Zn used for the starting mixture, and thus samples of various compositions might be directly prepared. However, somewhat substoichiometric amount of iron ( $(Mn+Zn):Fe=1.80$ ) was intentionally employed for the synthesis, which guarantees that hematite is not formed as a possible admixture.

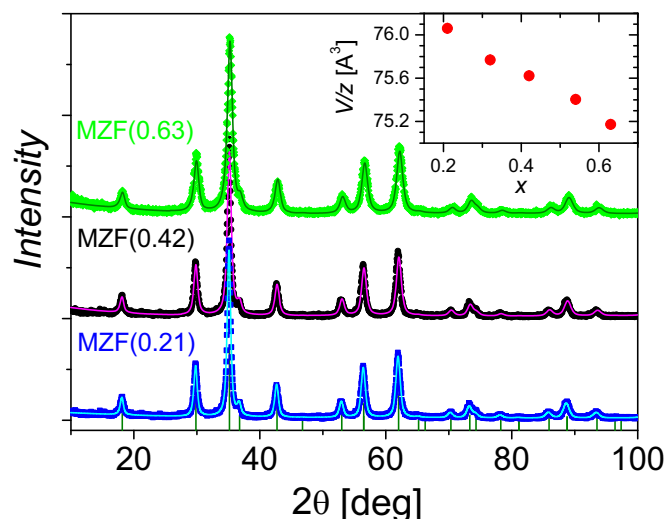


**Fig. 1.** X-ray diffraction patterns of selected samples of bare  $Mn_{1-x}Zn_xFe_2O_4$  cores, the vertical lines indicate reflections of the spinel phase with the  $Fd\bar{3}m$  symmetry. The inset shows the dependence of the unit cell volume per formula unit,  $V/z$ , on the content of zinc  $x$ .

**Table 1**

Chemical composition and structural properties of bare ferrite particles based on XRF and XRD measurements:  $y$  gives the stoichiometric content of Zn in the starting mixture,  $a$  is the lattice parameter of the cubic cell, and  $d_{XRD}$  designates the mean size of crystallites.

Sample	$y$	Composition	$a$ [Å]	$d_{XRD}$ [nm]
MZF(0.21)	0.20	$Mn_{0.82}Zn_{0.21}Fe_{1.97}O_4$	8.4739(4)	14
MZF(0.32)	0.30	$Mn_{0.69}Zn_{0.32}Fe_{1.99}O_4$	8.4632(4)	11
MZF(0.42)	0.40	$Mn_{0.61}Zn_{0.42}Fe_{1.97}O_4$	8.4576(4)	11
MZF(0.54)	0.50	$Mn_{0.52}Zn_{0.54}Fe_{1.94}O_4$	8.4495(5)	10
MZF(0.63)	0.60	$Mn_{0.42}Zn_{0.63}Fe_{1.95}O_4$	8.4408(3)	9

Similarly, the initial optimization of the procedure indicated that inert atmosphere during the adjustment of pH and following manipulation of the precursor is important to prevent undesired oxidation of Mn(II) in the oxide/hydroxide precipitates, that would lead to formation of hausmannite phases  $Mn_{3-x}Zn_xO_4$  or hematite as minor admixtures.

The ferrite cores of the composition  $Mn_{0.61}Zn_{0.42}Fe_{1.97}O_4$  were selected based on their magnetic properties (*vide infra*) for encapsulation into silica and subsequent studies. The morphology of the silica-coated sample, MZF(0.42)@silica, is shown by the transmission electron micrograph in Fig. 2a that provides important information on magnetic cores of the sample. The cores of coated particles, obtained by direct encapsulation of the as-prepared hydrothermal product, were predominantly formed by small clusters of ferrite crystallites, although an efficient stabilization by citrate had been applied prior to the deposition of silica.

The conclusive data were obtained by an extensive image analysis of TEM data carried out to determine the size distribution of whole coated particles ( $d_p$ ), their magnetic cores ( $d_c$ ), and individual crystallites ( $d_i$ ) in a spherical approximation. Histograms of the respective diameters together with selected descriptive statistics are shown in Fig. 2b. Generally, the observed size distribution of the diameters follows the log-normal distribution (see the fit in Fig. 2b). Further, both the direct inspection of large number of coated particles by TEM and the small overlap of the differential distribution functions of  $d_i$  and  $d_c$  indicate that the content of nanoparticles with single-crystalline cores is very low. Importantly, the volume-weighted mean size of crystallites inferred from TEM data,  $\bar{d}_{i,vw}=11$  nm corresponds to the mean size of crystallites of bare MZF(0.42) cores,  $d_{XRD}=11$  nm. Finally, the thickness of the silica shell, evaluated as a half of the difference between  $d_p$  and  $d_c$ , is described by a rather narrow distribution with the mean

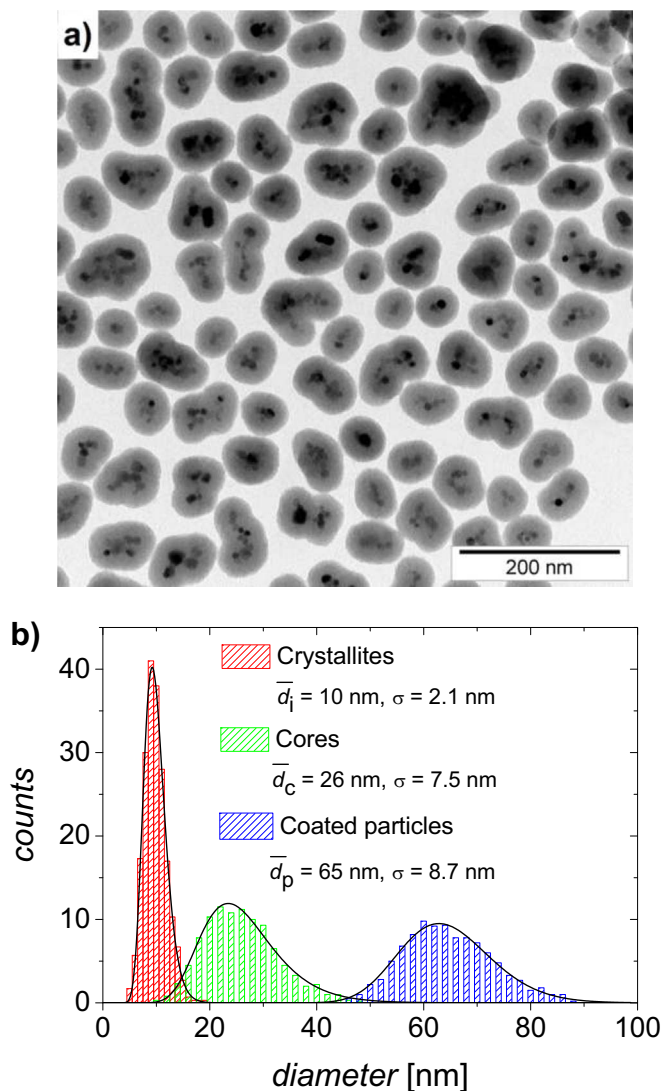


**Fig. 2.** TEM study of silica-coated  $\text{Mn}_{0.61}\text{Zn}_{0.42}\text{Fe}_{1.97}\text{O}_4$  ferrite particles: (a) micrograph showing that the magnetic cores consist predominantly of small clusters of  $\approx 10$  nm crystallites, (b) size distribution of whole coated particles ( $d_p$ ), their magnetic cores ( $d_c$ ), and individual crystallites ( $d_i$ ). The legend is supplemented by the mean diameters  $\bar{d}_j$  (where  $j=p, c$ , and  $i$ ), evaluated from experimental values, and the parameters  $\sigma_j$  of the lognormal distribution, i.e., the standard deviation of the natural logarithm of  $d_j$ . The volume-weighted mean diameters are  $\bar{d}_{j,vw} = 11, 31, 68$  nm for  $j=i, c, p$ , respectively, and the most frequent diameters (modes) are  $d_{j,max} = 9, 23, 63$  nm for  $j=i, c, p$ .

value of 19 nm and standard deviation of 1 nm.

### 3.2. Magnetic properties

The low- and room-temperature hysteresis loops of bare Mn-Zn ferrite cores, including also the measurement on coated particles  $\text{MZf}(0.42)\text{@silica}$ , are illustrated in Fig. 3. Generally, the magnetization of bare ferrite samples smoothly reaches saturation at comparable magnetic fields and is characterized by high values of  $M_{10\text{kOe}} = 72\text{--}107$   $\text{emu g}^{-1}$  at 5 K, decreasing to 23–65  $\text{emu g}^{-1}$  at 300 K (for the complete dependence of magnetization on the chemical composition see Fig. 4a).

All samples are ferrimagnetic due to antiferromagnetic interaction between spins on the tetrahedral and octahedral sublattices. Considering the strong preference of  $\text{Zn}^{2+}$  for tetrahedral sites, documented on bulk samples, a rather steep increase of net magnetic moment followed by certain maximum is expected to occur upon the substitution of manganese by zinc in the ferrite system. However, the

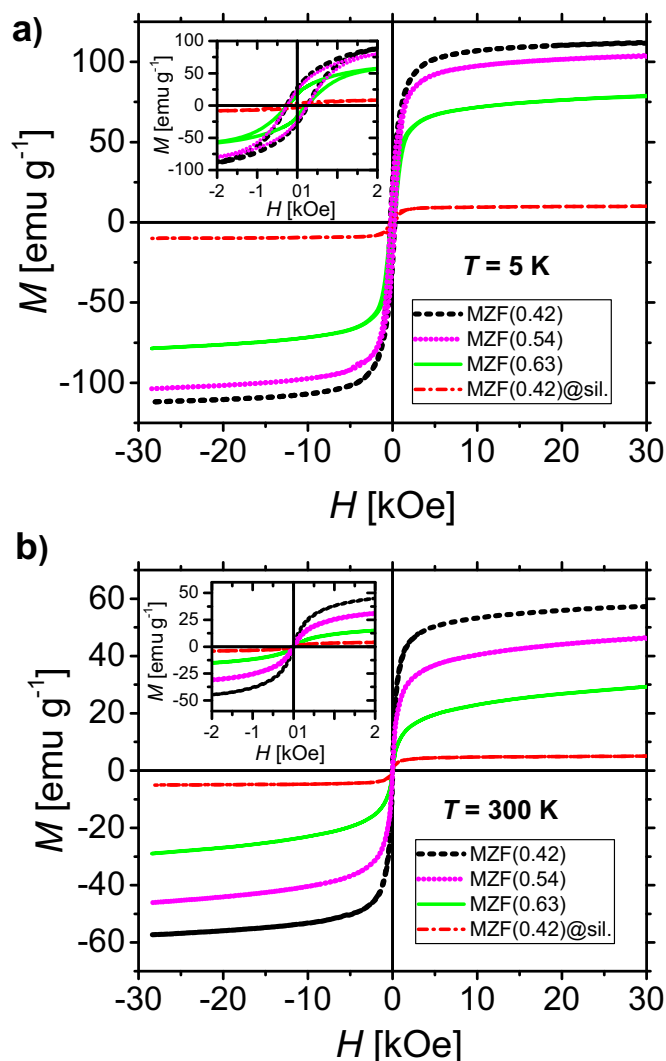


**Fig. 3.** Hysteresis loops of selected samples of bare  $\text{Mn}_{1-x}\text{Zn}_x\text{Fe}_2\text{O}_4$  cores and silica-coated  $\text{Mn}_{0.61}\text{Zn}_{0.42}\text{Fe}_{1.97}\text{O}_4$  particles at 5 K (a) and 300 K (b).

effect of zinc doping in nanoparticles is more complex. In the presently studied series of bare  $\text{MZf}(x)$  cores with  $x=0.21\text{--}0.63$ , the magnetization at low temperature exhibits a mild maximum at  $x=0.42$  (the magnetic moment per formula unit obtained through an extrapolation to zero field is  $m=4.55 \mu_B$ , see also Fig. 4b), after which a steep decrease is observed. Interestingly, both the samples with lower zinc content,  $x=0.21$  and  $0.32$ , show comparable moments as the  $\text{MZf}(0.42)$  cores, namely  $m=4.44$  and  $4.34 \mu_B$ .

A possible explanation might involve the fact that the cation distribution in the studied ferrite cores deviates from bulk systems, and non-zero occupancy of zinc on octahedral sites has to be considered. Such non-equilibrium cation distribution was evidenced in nanoparticles of Co-Zn ferrite prepared by a rather comparable procedure of coprecipitation followed by thermal treatment [26], and it was also suggested for Mn-Zn ferrite nanoparticles prepared by the hydrothermal route [24]. The metastable distribution in hydrothermal and coprecipitation products can be related to a rather low temperature of preparation (precipitation of a precursor at room temperature followed by hydrothermal treatment at  $180^\circ\text{C}$ ), combined with a very fast precipitation of precursors that occurs immediately after the adjustment of pH. On contrary, Mn-Zn ferrite nanoparticles as small as 15 nm, prepared by Jang et al. [7] by means of the thermal decomposition method (slow growth of nanocrystals at  $300^\circ\text{C}$ ), possessed the bulk-like cation distribution with almost negligible signal

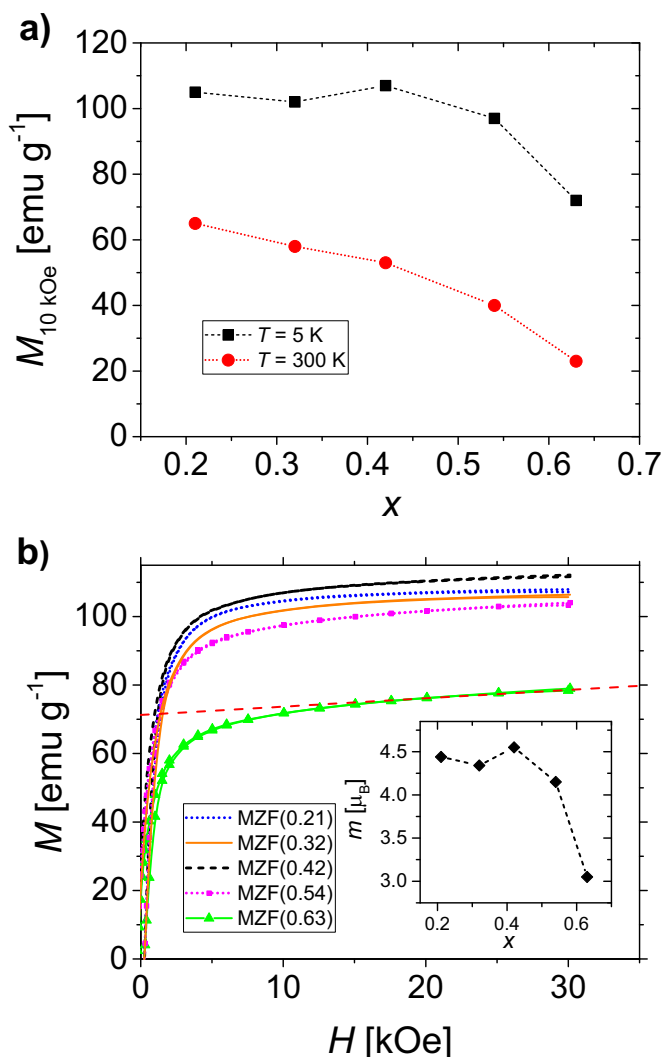


**Fig. 4.** Magnetization of bare  $\text{Mn}_{1-x}\text{Zn}_x\text{Fe}_2\text{O}_4$  ferrites cores in relation to the content of zinc: (a) low and room temperature magnetization at the magnetic field intensity  $H=10$  kOe, (b) magnetization curves at 5 K and the linear extrapolation of their high-field end (indicated by the dashed line for  $x=0.63$ ) to evaluate the magnetic moments of the ferrimagnetic ordering,  $m$  [ $\mu_B$  per formula unit] shown in the inset.

of  $\text{Zn}^{2+}$  on octahedral sites in an extended X-ray absorption fine structure (EXAFS) analysis. Moreover, these particles exhibited a sharp maximum of magnetization with respect to the zinc content at  $x=0.4$ .

The blocked state of bare particles at 5 K showed hysteresis with coercive fields in the narrow range of  $H_c=0.24$ – $0.26$  kOe. In contrast, the magnetization curves at 300 K revealed that the ferrite cores with higher zinc content were practically in superparamagnetic state at room temperature, although some small remanence was observed in all bare samples (from  $0.4$   $\text{emu g}^{-1}$  in MZF(0.21) to  $2.4$   $\text{emu g}^{-1}$  in MZF(0.63)). In order to get a better insight into the blocking behaviour of the prepared particles, ZFC-FC studies were carried out, and the temperature derivatives of the ZFC-FC susceptibility difference were analysed (see Fig. 5 for representative examples). The maximum of the so-obtained distribution of blocking temperatures for bare particles, that was generally rather broad, is formally described by the parameter  $T_{B,\max}\approx 80$ – $220$  K, whose dependence on the composition is shown in the inset of Fig. 5b. The main findings are as follows. At first, the distribution of blocking temperatures is shifted towards lower temperatures with increasing zinc content as the magnetocrystalline anisotropy decreases. Second, all the samples show at least a minor component of particles in the blocked state at room temperature, and its amount decreases with the content of zinc.

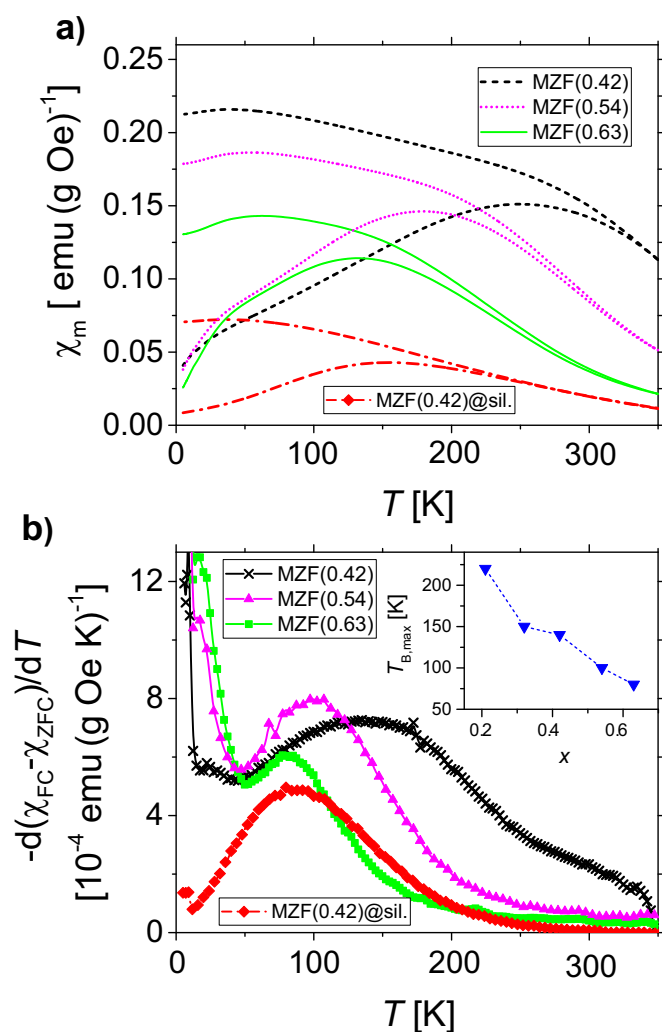


**Fig. 5.** Blocking behaviour of selected bare samples and coated nanoparticles MZF(0.42)@silica: (a) ZFC-FC susceptibility measurements at  $H=20$  Oe, (b) temperature derivative of the  $\chi_{FC}-\chi_{ZFC}$  susceptibility difference. The inset shows the dependence of the maximum of blocking temperature distribution,  $T_{B,\max}$ , on the zinc content,  $x$ , in the entire range of studied compositions.

Considering the magnetic behaviour of the different compositions, the  $\text{Mn}_{0.61}\text{Zn}_{0.42}\text{Fe}_{1.97}\text{O}_4$  sample seems to be a suitable candidate for MRI studies since these particles are almost completely superparamagnetic at physiological temperatures (in contrast to particles with lower  $x$ ), possess high magnetization of  $65$   $\text{emu g}^{-1}$  at 300 K (compared to samples with higher  $x$ ), and at the same time, these nanoparticles show a marked dependence of magnetization on temperature, which might be employed in the relaxometric analysis. The comparison of bare and silica-coated  $\text{Mn}_{0.61}\text{Zn}_{0.42}\text{Fe}_{1.97}\text{O}_4$  particles in Fig. 5 demonstrates a shift of blocking events to lower temperatures upon encapsulation into silica. Assuming a close-packed arrangement of the coated particles, the magnetic cores of  $\approx 25$  nm size are separated by  $\approx 38$  nm due to their silica shells, which practically confines the dipolar interactions among crystallites of individual silica-coated cores.

### 3.3. MRI related properties

The relaxometric measurements of aqueous suspension of MZF(0.42)@silica nanoparticles at the magnetic field  $B_0=0.5$  T revealed high transverse relaxivities with a pronounced temperature dependence (see Fig. 6). The relaxivity values determined at ambient and physiological temperatures were  $r_2(20^\circ\text{C})=450$   $\text{s}^{-1}$   $\text{mmol}(\text{Me}_3\text{O}_4)^{-1}$  L and  $r_2(37^\circ\text{C})=300$   $\text{s}^{-1}$   $\text{mmol}(\text{Me}_3\text{O}_4)^{-1}$  L,

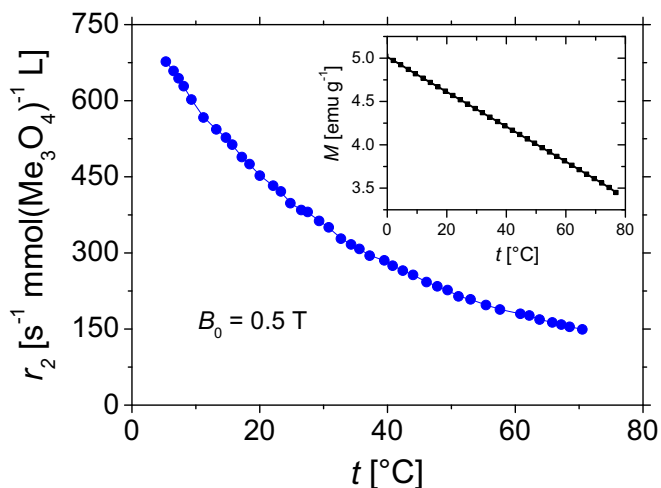


**Fig. 6.** Transverse relaxivity  $r_2$  of silica-coated  $\text{Mn}_{0.61}\text{Zn}_{0.42}\text{Fe}_{1.97}\text{O}_4$  ferrite cores at  $B_0=0.5$  T as a function of temperature. The inset shows the temperature dependence of the magnetization in the same magnetic field.

respectively, and thus exceeded even the performance of magnetic particles based on another type of complex oxides, specifically ferromagnetic  $\text{La}_{1-x}\text{Sr}_x\text{MnO}_3$  (LSMO) phases reported as promising contrast agents with extraordinary high  $r_2$ . In a detailed relaxometric study, silica-coated  $\text{La}_{1-x}\text{Sr}_x\text{MnO}_3$  nanoparticles of the composition  $x=0.20\text{--}0.45$  and higher  $d_{\text{XRD}}\approx 20$  nm exhibited values of  $r_2(20^\circ\text{C})=290\text{--}430\text{ s}^{-1}\text{ mmol}(\text{LSMO})^{-1}\text{ L}$  and  $r_2(37^\circ\text{C})=200\text{--}320\text{ s}^{-1}\text{ mmol}(\text{LSMO})^{-1}\text{ L}$ . The actual size of the coated LSMO particles was even higher ( $\bar{d}_c\approx 45$  nm and  $\bar{d}_p\approx 80$  nm) than in the present case of MZF(0.42)@silica nanoparticles ( $\bar{d}_c=26$  nm and  $\bar{d}_p=65$  nm, see Fig. 2b). The superior contrast properties of MZF(0.42)@silica should be discussed in relation to high magnetization of the employed magnetic phase ( $M_{10\text{K Oe}}(300\text{ K})=53\text{ emu g}^{-1}$ ) and the size of clusters that form its magnetic cores ( $\bar{d}_c=26$  nm). At the magnetic field of  $B_0=0.5$  T, these clusters, albeit composed of only 10 nm sized crystallites in superparamagnetic state (see the ZFC-FC study of the MZF(0.42)@silica sample in Fig. 5), achieve high magnetic moment comparable with the magnetic moment of a single magnetic particle of an equivalent volume. Consequently, higher transverse relaxivity (compared to well-dispersed crystallites) is observed up to a certain limit size of the cluster [10,11].

As regards the temperature dependence of the transverse relaxivity, it provides an interesting insight in the mechanism of transverse relaxation. The decrease of the relaxivity from  $r_2=680\text{--}170\text{ s}^{-1}\text{ mmol}(\text{Me}_3\text{O}_4)^{-1}\text{ L}$  in the studied range of  $5\text{--}70^\circ\text{C}$  can be empirically described by a quadratic function, whereas the decrease of the magnetization of MZF(0.42)@silica particles at  $B_0=0.5$  T from  $M=5.0\text{--}3.6\text{ emu g}^{-1}$  is practically linear (see the inset in Fig. 6). In a rough approximation, abstracting away from the cluster-based structure of magnetic cores, one might consider the theoretically predicted equation for relaxation rate in the motional averaging regime (MAR),  $R_2=16\tau_D(\Delta\omega)^2/45$ , where  $f$  is the volume fraction of magnetic nanoparticles,  $\tau_D=r^2/D$  is the characteristic diffusion time of water, depending on the distance of the closest approach  $r$  (i.e., the effective particle radius) and the self-diffusion coefficient of water  $D$ , and  $\Delta\omega$  represents the distribution of Larmor frequencies at the radius  $r$  [9,27]. The relation between  $\Delta\omega$  and volume magnetization of particles,  $M_V$ , can be described by the expression  $\Delta\omega = \mu_0\gamma M_V/3$ , where  $\mu_0$  is the permeability of free space and  $\gamma$  is the gyromagnetic ratio of  $^1\text{H}$  nuclei. The self-diffusion coefficient of water, increasing from  $1.303\cdot 10^{-9}\text{ m}^2\text{ s}^{-1}$  at  $5^\circ\text{C}$  to  $5.615\cdot 10^{-9}\text{ m}^2\text{ s}^{-1}$  at  $70^\circ\text{C}$ , shows also a significant temperature dependence, that can be fitted by the Speedy-Angell power law [28]. In contrast to MAR, the diffusion processes in the static dephasing regime are no more efficient in averaging out variations of magnetic fields

around particles; therefore, the relaxation rate approaches to the static limit described by the expression  $R_2^*=2\pi f\Delta\omega/27$ . Under these conditions, the relaxation rate is a linear function of magnetization and the diffusion component vanishes. Taking into account the observed dependence of transverse relaxivity of MZF(0.42)@silica nanoparticles on temperature, a predominant fraction of the sample probably acts in a MAR-like regime, where both the quadratic dependence of  $R_2$  on the magnetization and its inverse dependence on the self-diffusion of water decrease the value of transverse relaxivity with increasing temperature.

#### 4. Conclusions

Magnetic nanoparticles of  $\text{Mn}_{1-x}\text{Zn}_x\text{Fe}_2\text{O}_4$  ferrites in the compositional range of  $x\approx 0.2\text{--}0.6$  and with the mean size of crystallites  $\approx 10$  nm have been prepared by fast and facile procedure under hydrothermal conditions. Encapsulation of the as-prepared particles into silica has provided well-coated clusters of ferrite crystallites with the mean diameter of magnetic cores  $\approx 25$  nm.

Thorough magnetic characterizations carried out on bare samples suggest that cores with the composition of  $x\approx 0.4$  are suitable candidates for relaxometric studies since these particles are completely superparamagnetic at physiological temperatures, still retain high magnetization, and they also show marked dependence of the magnetization in a broad range around the physiological temperature.

The relaxometry at  $B_0=0.5$  T reveals that silica-coated clusters of  $\text{Mn}_{0.61}\text{Zn}_{0.42}\text{Fe}_{1.97}\text{O}_4$  provide high transverse relaxivity with a pronounced temperature dependence, specifically the values  $r_2(20^\circ\text{C})=450\text{ s}^{-1}\text{ mmol}(\text{Me}_3\text{O}_4)^{-1}\text{ L}$  and  $r_2(37^\circ\text{C})=300\text{ s}^{-1}\text{ mmol}(\text{Me}_3\text{O}_4)^{-1}\text{ L}$  were determined at room and body temperatures. The analysis of the temperature dependence indicates that the predominant fraction of the particles induce the transverse relaxation via a mechanism similar to the motional averaging regime.

#### Acknowledgement

The study was financially supported by the Czech Science Foundation through the project 16-04340S.

#### References

- [1] E. Pollert, P. Veverka, M. Veverka, O. Kaman, K. Závěta, S. Vasseur, R. Epherre, G. Goglio, E. Duguet, Search of new core materials for magnetic fluid hyperthermia: preliminary chemical and physical issues, *Prog. Solid State Chem.* 37 (2009) 1–14.
- [2] A.A. Kuznetsov, O.A. Shlyakhtin, N.A. Brusentsov, O.A. Kuznetsov, “Smart” mediators for self-controlled inductive heating, *Eur. Cells Mater.* 3 (Suppl. 2) (2002) S75–S77.
- [3] O. Kaman, P. Veverka, Z. Jiráček, M. Maryško, K. Knížek, M. Veverka, P. Kašpar, M. Burian, V. Šepelák, E. Pollert, The magnetic and hyperthermia studies of bare and silica-coated  $\text{La}_{0.75}\text{Sr}_{0.25}\text{MnO}_3$  nanoparticles, *J. Nanopart. Res.* 13 (2011) 1237–1252.
- [4] E. Pollert, K. Knížek, M. Maryško, P. Kašpar, S. Vasseur, E. Duguet, New  $T_C$ -tuned magnetic nanoparticles for self-controlled hyperthermia, *J. Magn. Magn. Mater.* 316 (2007) 122–125.
- [5] H. Rudolf, D. Silvio, M. Robert, Z. Matthias, Magnetic particle hyperthermia: nanoparticle magnetism and materials development for cancer therapy, *J. Phys. Condes. Matter* 18 (2006) S2919–S2934.
- [6] V. Herynek, K. Turnovcová, P. Veverka, T. Dědourková, P. Žvátora, P. Jendelová, A. Gálisová, L. Kosinová, K. Jiráčková, E. Syková, Using ferromagnetic nanoparticles with low Curie temperature for magnetic resonance imaging-guided thermoablation, *Int. J. Nanomed.* 11 (2016) 3801–3811.
- [7] J.T. Jang, H. Nah, J.H. Lee, S.H. Moon, M.G. Kim, J. Cheon, Critical enhancements of MRI contrast and hyperthermic effects by dopant-controlled magnetic nanoparticles, *Angew. Chem. Int. Ed.* 48 (2009) 1234–1238.
- [8] O. Kaman, T. Dědourková, J. Koktan, J. Kuličková, M. Maryško, P. Veverka, R. Havelek, K. Královec, K. Turnovcová, P. Jendelová, A. Schröfel, L. Svoboda, Silica-coated manganite and Mn-based ferrite nanoparticles: a comparative study focused on cytotoxicity, *J. Nanopart. Res.* 18 (2016) 100.
- [9] M.R.J. Carroll, R.C. Woodward, M.J. House, W.Y. Teoh, R. Amal, T.L. Hanley, T.G. Pierre St, Experimental validation of proton transverse relaxivity models for superparamagnetic nanoparticle MRI contrast agents, *Nanotechnology* 21 (2010) 035103.
- [10] Y. Matsumoto, A. Jasanoff,  $T_2$  relaxation induced by clusters of superparamagnetic nanoparticles: Monte Carlo simulations, *Magn. Reson. Imaging* 26 (2008)

- 994–998.
- [11] A. Roch, Y. Gossuin, R.N. Muller, P. Gillis, Superparamagnetic colloid suspensions: water magnetic relaxation and clustering, *J. Magn. Magn. Mater.* 293 (2005) 532–539.
- [12] T. Dědourková, O. Kaman, P. Veverka, J. Koktan, M. Veverka, J. Kuličková, Z. Jiráček, V. Herynek, Clusters of magnetic nanoparticles as contrast agents for MRI: the effect of aggregation on transverse relaxivity, *IEEE Trans. Magn.* 51 (2015) 5300804.
- [13] B. Jeyadevan, K. Tohji, K. Nakatsuka, A. Narayanasamy, Irregular distribution of metal ions in ferrites prepared by co-precipitation technique structure analysis of Mn-Zn ferrite using extended X-ray absorption fine structure, *J. Magn. Magn. Mater.* 217 (2000) 99–105.
- [14] R. Arulmurugan, B. Jeyadevan, G. Vaidyanathan, S. Sendhilnathan, Effect of zinc substitution on Co-Zn and Mn-Zn ferrite nanoparticles prepared by co-precipitation, *J. Magn. Magn. Mater.* 288 (2005) 470–477.
- [15] A. Chatterjee, D. Das, S.K. Pradhan, D. Chakravorty, Synthesis of nanocrystalline nickel-zinc ferrite by the sol-gel method, *J. Magn. Magn. Mater.* 127 (1993) 214–218.
- [16] R. Gimenes, M.R. Baldissera, M.R.A. da Silva, C.A. da Silveira, D.A.W. Soares, L.A. Perazolli, M.R. da Silva, M.A. Zaghete, Structural and magnetic characterization of  $Mn_xZn_{1-x}Fe_2O_4$  ( $x=0.2; 0.35; 0.65; 0.8; 1.0$ ) ferrites obtained by the citrate precursor method, *Ceram. Int.* 38 (2012) 741–746.
- [17] X.M. Liu, S.Y. Fu, Synthesis of nanocrystalline  $Zn_{0.5}Mn_{0.5}Fe_2O_4$  via in situ polymerization technique, *J. Magn. Magn. Mater.* 308 (2007) 61–64.
- [18] J. Xie, Y. Zhang, C.Y. Yan, L. Song, S. Wen, F.C. Zang, G. Chen, Q. Ding, C.Z. Yan, N. Gu, High-performance PEGylated Mn-Zn ferrite nanocrystals as a passive-targeted agent for magnetically induced cancer theranostics, *Biomaterials* 35 (2014) 9126–9136.
- [19] N.Z. Bao, L.M. Shen, W. An, P. Padhan, C.H. Turner, A. Gupta, Formation mechanism and shape control of monodisperse magnetic  $CoFe_2O_4$  nanocrystals, *Chem. Mater.* 21 (2009) 3458–3468.
- [20] Y.W. Jun, Y.M. Huh, J.S. Choi, J.H. Lee, H.T. Song, S. Kim, S. Yoon, K.S. Kim, J.S. Shin, J.S. Suh, J. Cheon, Nanoscale size effect of magnetic nanocrystals and their utilization for cancer diagnosis via magnetic resonance imaging, *J. Am. Chem. Soc.* 127 (2005) 5732–5733.
- [21] H. Yang, C.X. Zhang, X.Y. Shi, H. Hu, X.X. Du, Y. Fang, Y.B. Ma, H.X. Wu, S.P. Yang, Water-soluble superparamagnetic manganese ferrite nanoparticles for magnetic resonance imaging, *Biomaterials* 31 (2010) 3667–3673.
- [22] M. Zhang, B.L. Cushing, C.J. O'Connor, Synthesis and characterization of monodisperse ultra-thin silica-coated magnetic nanoparticles, *Nanotechnology* 19 (2008) 085601.
- [23] C. Rath, K.K. Sahu, S. Anand, S.K. Date, N.C. Mishra, R.P. Das, Preparation and characterization of nanosize Mn-Zn ferrite, *J. Magn. Magn. Mater.* 202 (1999) 77–84.
- [24] C. Rath, S. Anand, R.P. Das, K.K. Sahu, S.D. Kulkarni, S.K. Date, N.C. Mishra, Dependence on cation distribution of particle size, lattice parameter, and magnetic properties in nanosize Mn-Zn ferrite, *J. Appl. Phys.* 91 (2002) 2211–2215.
- [25] P. Veverka, O. Kaman, M. Kačenka, V. Herynek, M. Veverka, E. Šantavá, I. Lukeš, Z. Jiráček, Magnetic  $La_{1-x}Sr_xMnO_3$  nanoparticles as contrast agents for MRI: the parameters affecting  $^1H$  transverse relaxation, *J. Nanopart. Res.* 17 (2015) 33.
- [26] M. Veverka, Z. Jiráček, O. Kaman, K. Knížek, M. Maryško, E. Pollert, K. Závěta, A. Lančok, M. Dlouhá, S. Vratislav, Distribution of cations in nanosize and bulk Co-Zn ferrites, *Nanotechnology* 22 (2011) 345701.
- [27] R.A. Brooks,  $T_2$ -shortening by strongly magnetized spheres: a chemical exchange model, *Magn. Reson. Med.* 47 (2002) 388–391.
- [28] M. Holz, S.R. Heil, A. Sacco, Temperature-dependent self-diffusion coefficients of water and six selected molecular liquids for calibration in accurate  $^1H$  NMR PFG measurements, *Phys. Chem. Chem. Phys.* 2 (2000) 4740–4742.